JOURNAL OF MATERIALS SCIENCE 17 (1982) 1479–1486

Grain-boundary segregation in an Al–8 wt % Mg alloy

T. MALIS*, M. C. CHATURVEDI†
Alcan International Ltd, Kingston Laboratories, Kingston, Ontario, Canada

The grain-boundary segregation of Mg atoms in a high-purity Al–8 wt% Mg alloy, water quenched from the solution heat-treatment temperature, has been investigated by energy dispersive X-ray microanalysis in a TEM/STEM electron microscope. Many grain boundaries showed a segregation of Mg atoms to a level 2 to 3 times higher than the alloy composition. In the as-quenched state, Mg was uniformly distributed along the grain boundaries, but formed clusters during ageing at room temperature. Hydrogen bubbles were often associated with these Mg-rich regions. Mg-depleted zones were observed adjacent to most boundaries, but in most cases on only one side of the boundary.

1. Introduction

The grain-boundary segregation of Mg on water quenching Al–Zn–Mg alloys from their solution heat-treatment temperature has been suggested as one of the major factors making them stress-corrosion susceptible [1–3]. However, the existence of such a segregation has not been unambiguously established. For example, Chen *et al.* [1] have observed segregation of Mg at the grain boundaries of water-quenched and aged Al–Zn–Mg alloy by Auger electron spectroscopy, but it was not detected by energy dispersive X-ray microanalysis (EDS) [4, 5] and electron energy-loss spectroscopy (EELS) [6] techniques. In the as-quenched conditions, however, Mg and Zn enriched grain boundaries have been observed by electron micro-probe [7], EELS [8] and oxide replica [9] techniques. In an Al–7 wt% Mg alloy Cundy *et al.* [10] using EELS technique observed a depletion of Mg at the grain boundaries. However, the work of Scamans and Rehal [11] suggests the Mg enrichment of grain boundaries in solution heat-treated and water quenched Al–5 wt% Mg and Al–4.3 wt% Zn–1.5 wt% Mg alloys. Their conclusion is based on the observation that the addition of Mg to Al and Al–Zn alloy caused a preferential reaction at the grain boundaries–surface intersection when these alloys were exposed to water vapour saturated air at 70° C. It should also be noted that they did not observe any Mg enrichment of the grain boundary by EDS technique in a TEM/STEM microscope. The inability of the EDS technique to detect segregation of Mg may be, (a) due to Mg being an inefficient source of X-rays and/or (b) due to the small amount of Mg being generally present in those alloys that have been studied by this technique. Therefore, to study the influence of water quenching from the solution heat-treatment temperature on the distribution of Mg atoms it was decided to investigate a more concentrated, i.e., Al–8 wt% Mg alloy using the EDS technique.

2. Experimental technique

2.1. Specimen preparation

An Al–8.0 wt% Mg alloy was prepared in an air furnace using high-purity alloying elements and cast in a permanent mould. The actual magnesium content was 8.37 wt% and the total usual metallic impurity was less than 0.01 wt%. The ingot was hot and cold-rolled to a 1.0 mm thick sheet, then given a final solution heat-treatment of 1 h at 350° C and water quenched. The structure of the solution heat-treated sheet was equiaxed grains which were 20 μm in diameter. Some material was aged for up to several weeks either at room

*Present address: Physical Metallurgy Research Laboratory, CANMET, Ottawa, Ontario, Canada.
†Present address: Department of Mechanical Engineering, University of Manitoba, Winnipeg, Manitoba, Canada.

0022–2461/82/051479–08$03.46/0

temperature (22° C) or in a freezer (− 5° C). Thin foils for electron microscopy were prepared by a standard dual-jet electropolishing technique using 20% perchloric–ethanol bath at − 10° C and 15 V.

2.2. X-ray microanalysis

The structural examination and microanalysis of thin foils was carried out in a Philips EM400 electron microscope equipped with a STEM unit and EDAX 9100/60 EDS facilities. The microscope was also equipped with special apertures to limit spurious X-ray production to a minimum [12] and a Be-insert low-background specimen holder was used.

The thin foil thickness, determined from contamination spot spacings [13], was always between 100 and 300 nm, and both absorption and fluorescence corrections were ignored [14]. A nominal electron-beam diameter of 20 nm in the STEM mode was used for the microanalysis which, due to beam broadening in 100 to 300 nm thick foils would result in an actual beam diameter of about 30 to 40 nm [14]. The grain boundaries analysed were usually edge-on to the electron beam at the tilt angle of 20° necessary for X-ray analysis, i.e., the projected width of the grain boundaries in the image plane was less than the broadened beam diameter. The preset analysis value of integrated area under the peak was generally 1000 MgKα X-ray counts, which required a counting time of 50 to 100 sec and did not cause any detectable specimen drift. The statistical uncertainty in the measurement for a single standard deviation for 1000 count preset was estimated to be about ± 3%. Another source of error in the grain-boundary analysis could have resulted from the electron beam not being centred exactly on the boundary. Assuming a 1 nm thick segregate film on an exactly edge-on boundary, this error will have a maximum value of ± 4.0%. If the boundary was inclined or if the film was thicker, this positional error would be substantially reduced. Since Al- and MgKα peaks overlap to a certain extent, an overlap correction factor was also determined periodically. It was always found to be 0.65% and was applied to the integrated peak intensities. To minimize the error in the measurements due to the complex shape of the continuum background underlying Al- and MgKα peaks, the same background was subtracted from each X-ray spectrum.

3. Results

3.1. Grain-boundary structure

The grain-boundary structure of freshly solution-treated and water-quenched specimens, as well as of those aged at 22° C and − 5° C, were examined by transmission electron microscopy (TEM). The grain-boundary structure of a freshly solution-treated and water-quenched specimen was typical of a recrystallized solid solution, i.e., a few grain boundaries were defect-free while others had both intrinsic and extrinsic dislocations on them. This remained unchanged for the first few days of ageing at 22° C, but after several days a large number of boundaries developed bubbles. At the longer ageing times, about two thirds of the boundaries showed extensive bubble formation. A typical example of bubbles in a specimen aged at room temperature is shown in a triple-point collage in Fig. 1. The boundaries were examined at high magnifications over large angles of tilt under various diffracting conditions, yet no evidence of precipitation was detected. Therefore, it was concluded that the bubbles were molecular hydrogen [15–17]. As illustrated by Fig. 1, both the size and distribution of bubbles varied from boundary to boundary, the former generally being 8 to 100 nm. As has been reported earlier [15–17], the electron beam seemed to facilitate the nucleation and growth of hydrogen bubbles; however, in some well-aged specimens bubbles were observed immediately upon examination. This would suggest that the bubbles in such specimens could have formed during ageing at room temperature and were not nucleated solely by the electron beam. On a few grain boundaries, growth of bubbles, as illustrated in Fig. 2, was continued under *in situ* electron-beam heating until they coalesced, resulting in the decohesion of the boundary and disappearance of the strain fields. Boundaries similar in appearance to Fig. 2a and c were observed, suggesting a process of extensive bubble growth leading to "serrated" boundaries, as exemplified by Fig. 3. It should, however, be noted that some foils were examined at different ageing times and that the size of hydrogen bubbles on most boundaries did not change substantially, even after ageing for up to three months at room temperature. A few grain boundaries in extensively-aged foils were also seen to be heavily pitted, as shown in Fig. 4, which could be due to preferential anodic dissolution, as has been reported earlier [16].

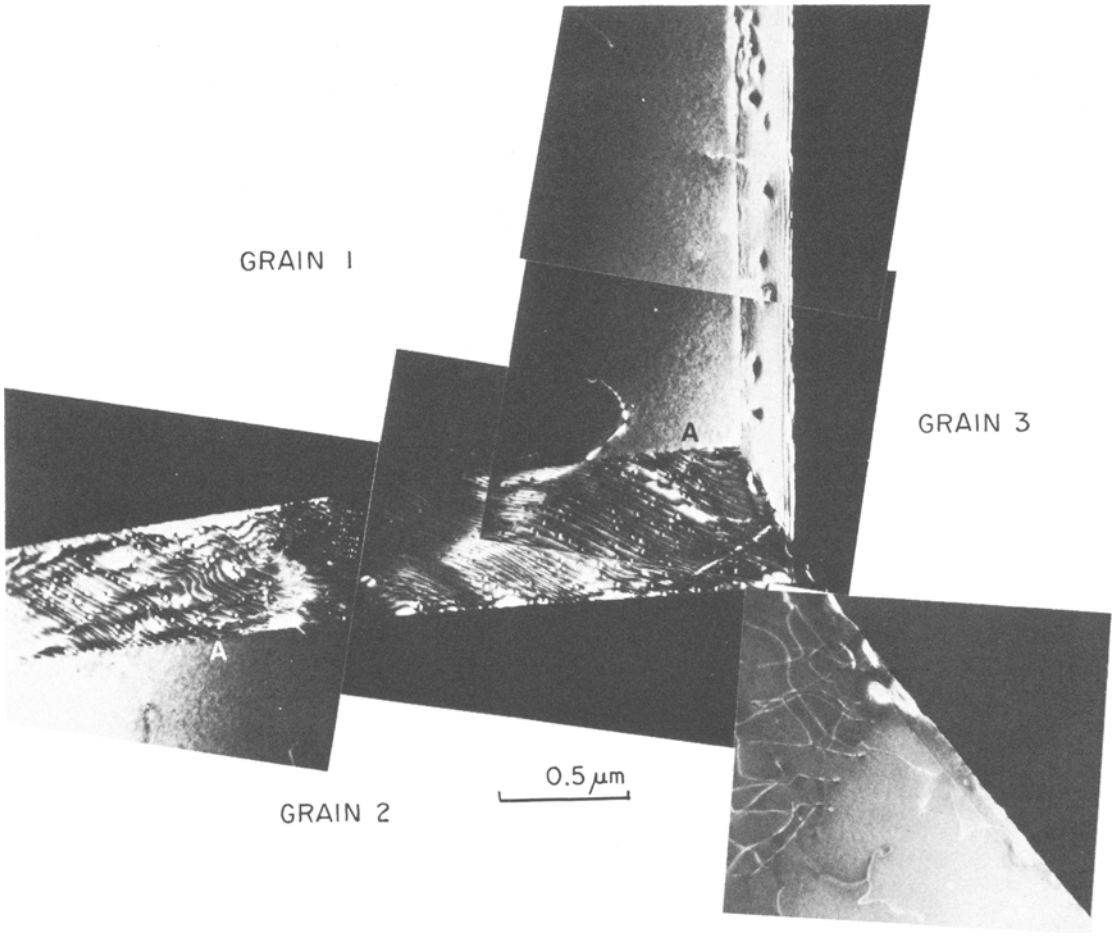

Figure 1 Dark-field collage of a grain-boundary triple-point showing variation in hydrogen bubble size and distribution. Boundary 1–2 contains two intrinsic dislocation networks, one with small bubbles on it and the other barely visible at points such as A.

3.2. X-ray microanalysis

The X-ray microanalysis of 28 grain boundaries and adjacent grain interiors was carried out to determine the distribution of Mg atoms. The microanalysis was normally carried out in the form of a trace consisting of 10 or more point analyses about 100 nm apart along the grain boundary and, for a few boundaries, another parallel trace about 1000 nm from the boundary. Some analytical traces were also conducted normal to the grain boundary into the neighbouring grains. The X-ray spectrum from each point was processed and the concentration of Mg was expressed as the ratio of Mg- and AlKα integrated peak areas. Each analytical trace consisting of several point analyses was characterized by a mean variation in Mg/Al ratio and its standard deviation.

Table I shows the results of representative analytical traces conducted within a number of grain centres. It is seen that the variation along the trace, as reflected by the standard deviation lies approximately within the range of X-ray statistical uncertainty. For the grain interiors adjacent to boundaries, a total of 17 traces had an average deviation of 3.5%, indicating no substantial differences from the grain centres. Thus, comparisons to boundary traces were normally conducted by single-area scans in each grain, as in Table II, which shows the data for the 28 boundaries studied. The

TABLE I Grain centre microanalysis data

Mean Mg/Al ratio	Standard deviation (%)
6.9	3.4
7.2	3.2
7.2	3.4
7.2	2.9

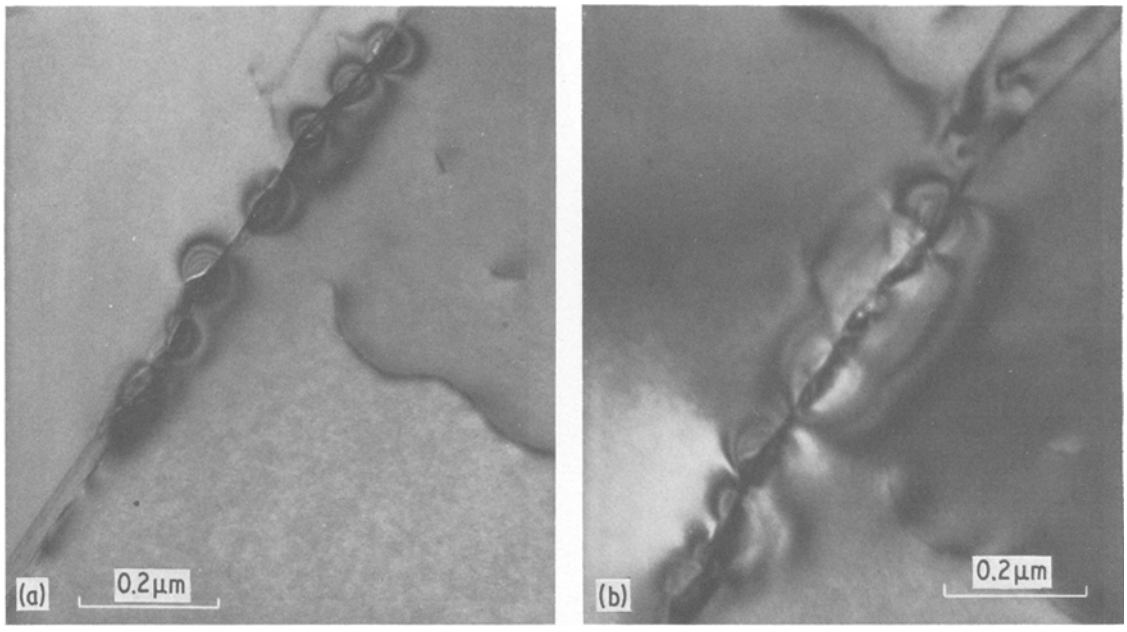

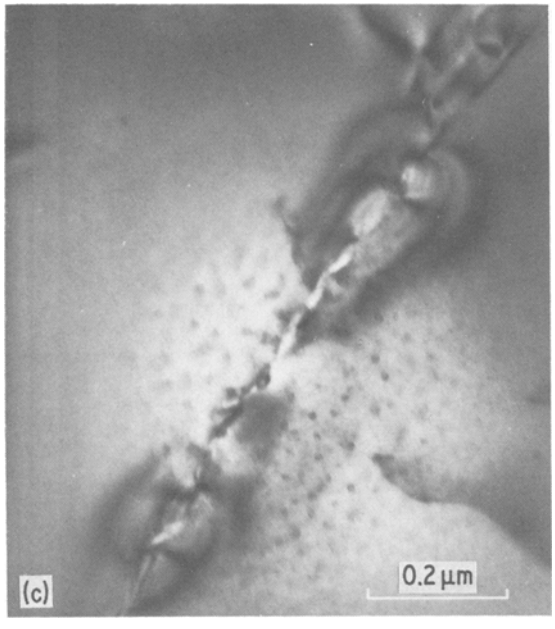

Figure 2 Accelerated bubble growth due to electron-beam heating. (a) Bubbles as observed upon examination of an aged specimen; (b) after 2 min of beam heating with all apertures removed; (c) after 7 min of heating (note decrease in strain contrast and increase in boundary decohesion).

grains adjacent to each boundary normally had identical Mg/Al ratios, a few showed slightly different values and an average value is listed in Table II. For each boundary–grain pair, a meaningful difference was regarded as one where the mean Mg/Al value for the boundary trace lay outside the uncertainty range (± 3.5%), of the value for the adjacent grain interiors, i.e., above ± 3.5%. Thus, 4 of the 7 as-quenched boundaries showed significant differences along with 13 of the 21 boundaries in aged material. While the great majority indicated Mg enhancement, a few also showed net depletion.

The entire set of boundary and grain interior values were also tested statistically, and both correlation and null hypothesis tests indicated a high probability of a significant average difference between grain boundaries and grain interiors. The as-quenched boundaries had an average variation (standard deviation) along the trace of 4.8% as opposed to the average value of 3.5% for grain interiors. The difference is likely a reflection of the positional uncertainty of the electron beam for boundary analysis. Boundaries in aged material which had few or no bubbles possessed an average deviation of 6% while those which were heavily-bubbled and/or serrated had an average deviation of 25%, indicating an increased Mg variation along the boundary both with ageing and the appearance of bubbles.

Finally, a few boundaries had more than one trace conducted on them, and variations from segment to segment similar to variations in bubble distribution were observed.

An illustration of the variation of both Mg and

TABLE II Mg/Al ratios for boundaries and adjacent grains

Condition	Boundary	Adjacent grains (average)
As-quenched	7.6 ± 4.4%	7.45
	7.4 ± 4.4%	7.35
	8.0 ± 5.1%	8.0
	6.3 ± 8.5%	6.6
	8.0 ± 3.0%	7.55
	8.4 ± 4.0%	7.8
	7.1 ± 4.0%	6.65
Aged showing few or no bubbles	7.1 ± 3.0%	7.05
	6.6 ± 5.8%	6.65
	7.2 ± 4.8%	7.3
	7.5 ± 5.9%	7.3
	7.6 ± 7.3%	7.5
	6.8 ± 5.4%	6.7
	6.9 ± 7.5%	7.0
	7.2 ± 7.7%	7.65
	7.7 ± 6.8%	7.0
	7.4 ± 4.3%	7.0
	8.0 ± 5.1%	7.6
	7.5 ± 3.7%	6.95
	7.4 ± 6.2%	6.95
	7.2 ± 6.4%	6.9
	7.5 ± 7.1%	7.2
	7.2 ± 9.7%	6.8
Aged showing many bubbles/ "serrated"	6.2 ± 10.4%	7.4
	6.4 ± 40.0%	7.0
	7.4 ± 18.0%	6.8
	7.1 ± 39.0%	6.9
	7.4 ± 18.0%	6.8

bubbles from boundary to boundary is shown in Fig. 5. Boundary 1–3 (in Fig. 5) was free of bubbles and its analytical trace was very similar to that of the adjacent grain in both mean Mg/Al value and variation along the trace, as seen in Fig. 6. The trace on Boundary 2–3, which was heavily-bubbled, was different in both respects, as seen in Fig. 7a and b, with the Mg/Al peaks along the trace approximately corresponding to points where large bubbles were located. It was also observed that neither the average value of Mg/Al ratio nor the trace profile changed substantially when the foil was examined 2 months later. Boundary 1–2 had a high density of hydrogen bubbles on it but, unfortunately, its orientation was not suitable for microanalysis. However, other boundaries with a similar hydrogen bubble distribution generally showed a uniform net increase in Mg/Al ratio over that of the grain interior. Point analyses on individual large bubbles on inclined boundaries showed them to have a higher Mg/Al ratio than the neighbouring bubble-free area, with the ratio being greater the larger the bubble. A few more detailed analyses suggested that the highest Mg enrichment lay adjacent to, rather than directly over, the centre of the bubble strain field.

The analytical traces conducted normal to the Mg-enriched grain boundaries generally showed a

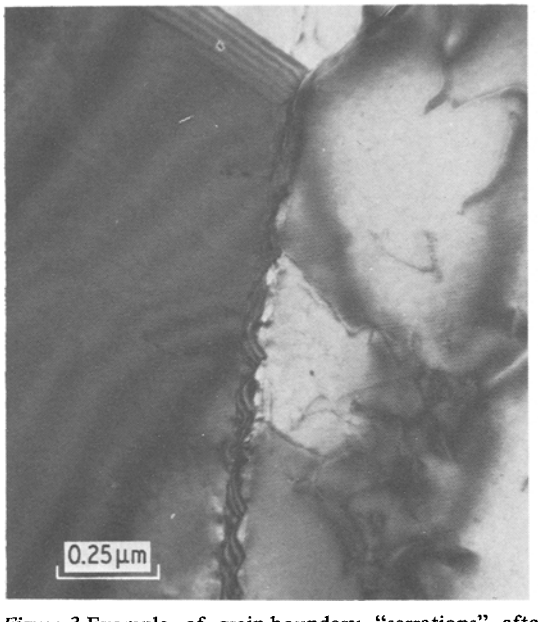

Figure 3 Example of grain-boundary "serrations" after extensive bubble growth.

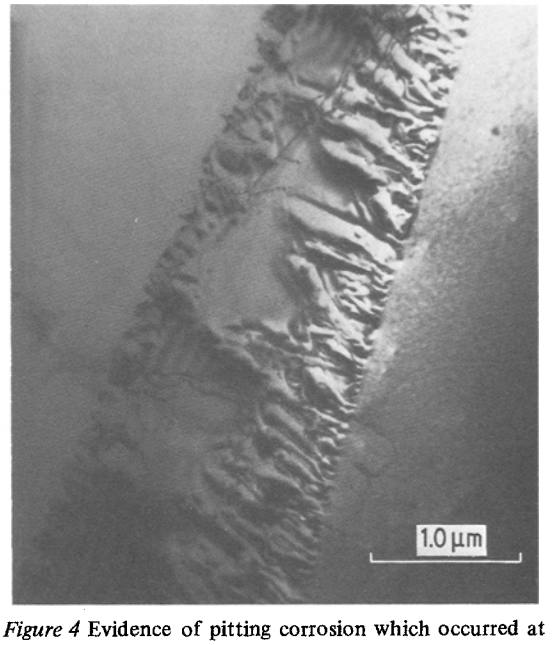

Figure 4 Evidence of pitting corrosion which occurred at a few grain boundaries in well-aged material.

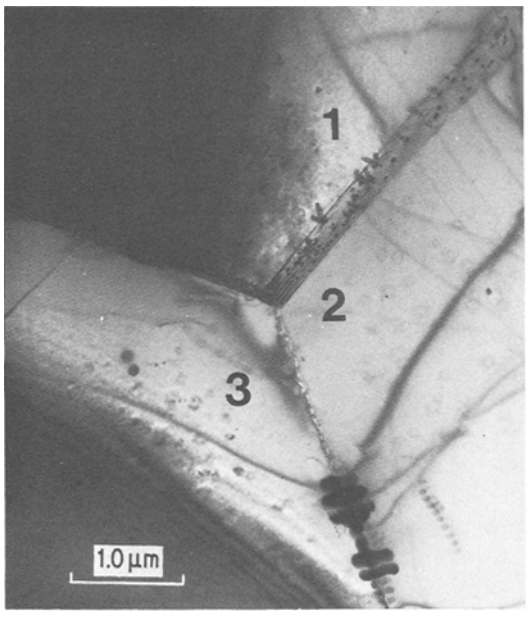

Figure 5 Triple-point illustrating varying bubble distributions and a varying Mg distribution, as shown in Figs 6 and 7.

solute-depleted zone extending to within several nanometers of the boundary, which was often present only on one side of the grain boundary. Two such traces conducted across Boundary 2–3 shown in Fig. 5 are shown in Fig. 7c and d. Furthermore, an analytical trace conducted within Grain 2 at a distance of 100 nm and parallel to the Boundary 2–3 also showed a uniform decrease in Mg/Al ratio as compared to both the grain interior and the grain boundary, i.e., a uniform solute-depleted zone. However, Grain 3 did not show a similar zone, having a mixture of enhancement, depletion and no change along a similar trace.

4. Discussion

The above results show that on water-quenching from the solution treatment temperature of 350° C some of the grain boundaries in this alloy become enriched with Mg solute atoms. The average Mg concentration at the enriched grain boundaries can be estimated by using the Cliff–Lorimer [18] technique of quantitative thin foil analysis. A K-factor value of 1.18 was determined by using the average value of the ratio of the MgKα and AlKα radiations from all the grain interior measurements and the composition of the alloy. Assuming a segregate film thickness of 2 to 3 nm [2] and taking beam broadening and solute-depleted zones into account, the average Mg concentration at the enriched grain boundaries in freshly solution treated and water-quenched specimens was estimated to be as high as 20 to 30 wt%. This is in agreement with the two-to-three fold increase observed by Chen *et al.* [1] in Al–Zn–Mg alloys and supports the conclusions arrived at by Auger spectroscopic studies [1, 3]. Thus, the Mg enrichment at grain boundaries in water-quenched material could be due to the presence of a supersaturation of quenched-in vacancies leading to vacancy–solute pair diffusion to boundaries [2]. The data suggests that low-temperature ageing leads to clustering of Mg at irregularly-spaced points along the boundary and that, when the local Mg concentration reaches a certain value, hydrogen bubbles can be nucleated and rapidly grow to a size which could be governed by a number of interrelated factors such as cluster size, the presence of boundary defects or the local supply of atomic hydrogen. It should be noted that a problem with the more heavily-bubbled/

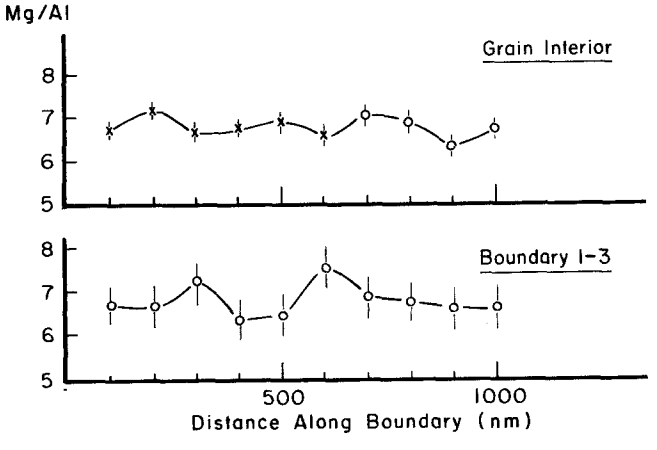

Figure 6 Grain interior and grain-boundary Mg/Al traces for the boundary between Grains 1 and 3 of Fig. 5. Boundary, 6.8 ± 5.4%; Grain, 6.7 ± 3.3%. X, 40 nm nominal beam diameter; 0, 20 nm nominal beam diameter.

serrated boundaries is that of varying foil thickness, especially if thin foil surface film effects, such as enriched oxides, are present [19]. However, there were no indications of such films, and, in any event, they could not have produced the observed Mg variations at and near bubbles. As noted earlier, it is highly likely that absorption and fluorescence corrections which are negligible in full foil thicknesses, are also minimal in the reduced thicknesses at bubbles.

The variation in Mg-concentration along the Mg-enriched boundaries in the aged specimens can be compared with recent observations by Gronsky and Furrer [20]. They observed that, on ageing an Al–Zn–Mg alloy, a high density of $MgZn_2$ particles, 20 to 30 nm in diameter, formed on both the intrinsic and extrinsic grain-boundary dislocations. Also, regions of high curvature or "serrations" in the grain boundary, similar to those seen in Fig. 3, were present at the grain-boundary precipitates which were about 100 nm in size. However, low-energy boundaries had very few precipitates on them. This could be because vacancy and solute movement to such low-energy boundaries would be extremely limited [21]. Therefore, it is likely that some of the bubble-free and non-enriched boundaries observed during the present investigation are of low energy type. The appearance of hydrogen bubbles on dislocations, as in Fig. 1, since bubbles are also associated with the sites of Mg enrichment, would indicate the segregation of Mg atoms to dislocations in the grain boundaries. Therefore, the solution-treatment temperature will not only influence the concentration of the quenched-in vacancies, which can influence the general migration of solute atoms to the grain boundaries, but will affect as well the defect structure, both intrinsic and extrinsic, of individual boundaries. This may produce the variation in Mg and bubbles from boundary to boundary.

The reasons for the association of Mg-rich regions and hydrogen bubbles in the aged material could not be established unambiguously. It is possible that the Mg and hydrogen atoms exist as a Mg–H complex and, when Mg atoms form clusters at defects in the grain boundaries on ageing, the hydrogen atoms combine together to

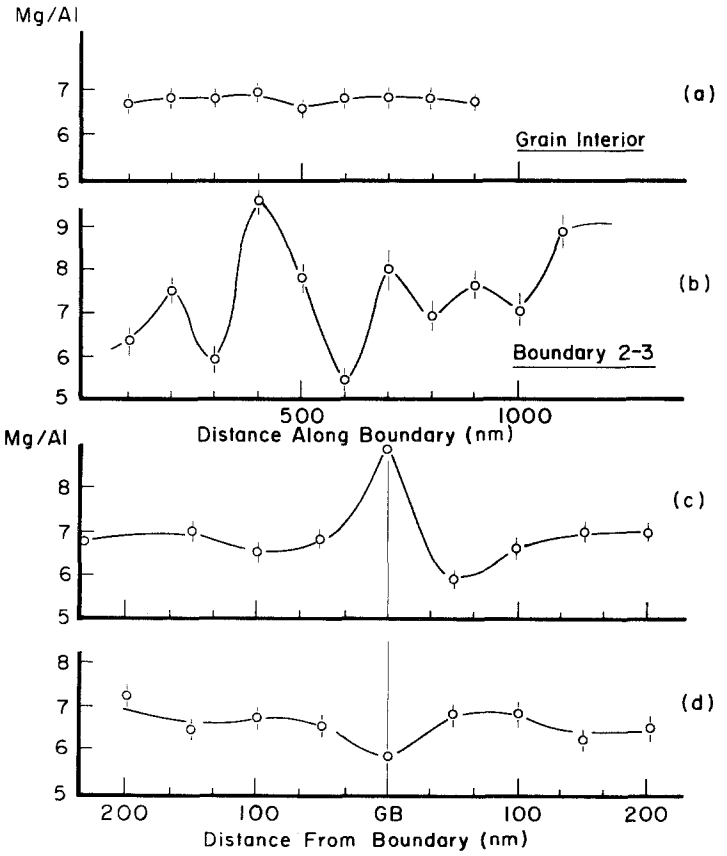

Figure 7 Grain interior and grain-boundary Mg/Al traces for boundary between Grains 2 and 3 of Fig. 7. (a) Grain interior trace, 6.8 ± 1.7%; (b) trace along the grain boundary, 7.4 ± 16.9%; (c and d) traces normal to the boundary approximately 100 nm apart.

form molecular hydrogen, as observed during the present investigations. This process would continue until the supply of hydrogen is exhausted. Hydrogen can enter this alloy during:

(i) melting and casting,

(ii) solution heat-treatment and water-quenching and

(iii) from the laboratory air.

Finally, the distinction between Mg-rich regions and actual precipitates is emphasized by the fact that boundary precipitates were seen in a few foils aged for some weeks at 22° C. Not only were these clearly visible under various diffraction conditions, but the Mg/Al ratios were some 50% higher than for the most enriched bubbles.

5. Conclusions

(a) In Al–8 wt% Mg alloy, water-quenched from 350° C, Mg atoms segregate at many grain boundaries. The extent of segregation varies from boundary to boundary and can range as high as 20 to 30 wt%. In the as-quenched condition, the Mg atoms are uniformly distributed along the grain boundaries.

(b) On room-temperature ageing a marked variation in the distribution of Mg along the enriched grain boundaries is observed, resulting in irregularly spaced, Mg-rich regions. The presence of precipitates was not detected until long after the appearance of this variation.

(c) In aged specimens these regions are often marked by the presence of hydrogen bubbles. These bubbles, generally, do not grow significantly with ageing time; however, after a prolonged ageing of thin films some of them disappear from the boundary as they intersect the foil surface.

(d) The presence of closely-spaced hydrogen bubbles can lead to the decohesion of grain boundaries.

(e) A Mg-depleted zone adjacent to the grain boundaries was usually observed, but often only in one grain.

Acknowledgements

The authors would like to thank Alcan International Limited, Kingston Laboratories, for providing the research facilities and permission to publish this work. Thanks are also due to Miss H. Lagacé and Mr H. Huff for technical assistance and Drs D. J. Lloyd and W. Tyson for many useful discussions. One of the authors (MCC) would also like to thank the University of Manitoba, Winnipeg, for granting him sabbatical leave.

References

1. J. M. CHEN, T. S. SUN, R. K. VISWANADHAM and J. A. S. GREEN, *Met. Trans.* **8A** (1977) 1935.
2. R. K. VISWANADHAM, T. S. SUN and J. A. S. GREEN, *ibid.* **11A** (1980) 85.
3. T. S. SUN, J. M. CHEN, R. K. VISWANADHAM and J. A. S. GREEN, *Appl. Phys. Lett.* **31** (1977) 580.
4. P. DOIG, P. E. J. FLEWITT and J. W. EDINGTON, *Corrosion* **33** (1977) 217.
5. M. RAGHAVAN, *Met. Trans.* **11A** (1980) 993.
6. P. DOIG and J. W. EDINGTON, *Corrosion* **31** (1975) 347.
7. C. R. SHASTRY and G. JUDD, *Met. Trans.* **3** (1972) 779.
8. P. DOIG and J. W. EDINGTON, *ibid.* **6A** (1975) 943.
9. I. T. TAYLOR and R. L. EDGAR, *ibid.* **2** (1971) 833.
10. S. L. CUNDY, A. J. F. METHERELL, M. J. WHELAN, P. N. T. UNWIN and R. B. NICHOLSON, *Proc. Roy. Soc.* **307A** (1968) 267.
11. G. M. SCAMANS and A. S. REHAL, *J. Mater. Sci.* **14** (1979) 2459.
12. N. J. ZALUZEC, "Introduction to Analytical Electron Microscopy (Plenum Press, New York, 1980) p. 121.
13. G. W. LORIMER, G. CLIFF and J. N. CLARK, in "Developments in Electron Microscopy and Analysis, EMAG '75" edited by J. A. Venables (Academic Press, London and New York, 1976) p. 153.
14. J. I. GOLDSTEIN, in "Developments in Electron Microscopy and Analysis, EMAG '75" edited by J. A. Venables (Academic Press, London and New York, 1976) p. 12.
15. L. CHRISTODOLOU and H. M. FLOWER, *Acta Met.* **28** (1980) 481.
16. R. ALANI and P. R. SWANN, *Brit. Corrosion J.* **12** (1977) 80.
17. G. M. SCAMANS, *J. Mater. Sci.* **13** (1978) 27.
18. G. CLIFF and G. W. LORIMER, *J. Microscopy* **103** (1975) 203.
19. P. L. MORRIS, N. C. DAVIES and J. A. TREVERTON, *Institute of Physics Conference Series* No. 36 (Institute of Physics, London, 1977) p. 377.
20. R. GRONSKY and P. FURRER, *Met. Trans.* **12A** (1981) 121.
21. R. W. BALLUFFI, "Grain Boundary Structure and Kinetics" (American Society of Metals, Metals Park, Ohio, 1980) p. 297.

Received 24 June
and accepted 16 October 1981